Line-narrowed fluorescence spectra and site-dependent transition probabilites of Nd^{3+} in oxide and fluoride glasses*

C. Brecher and L. A. Riseberg
GTE Laboratories, Inc., Waltham, Massachusetts 02154

M. J. Weber
Lawrence Livermore Laboratory, University of California, Livermore, California 94550
(Received 8 June 1978)

The fluorescence spectra, branching ratios, and decay of the $^4F_{3/2}$ state of Nd^{3+} in glass were measured under excitation by tunable pulsed laser radiation. The following glass types were studied: silicate, phosphate, borate, fluoroberyllate, and fluorophosphate. Measurements were made at liquid-helium temperatures by exciting into the $^2P_{1/2}$ state, and line-narrowed fluorescence spectra were obtained as a function of excitation wavelength. Large variations in Stark splitting of the $^4I_{9/2}$ and $^4I_{11/2}$ states have been observed and attributed to site-to-site differences in the local crystal field. The probabilities for radiative decay and for nonradiative decay by multiphonon emission also exhibit variations with excitation wavelength. Although similarities exist, each different glass type shows its own distinctive patterns of variation in crystal-field splitting and relative quantum efficiency. In the fluorophosphate glass, which contains large numbers of both fluorine and oxygen anions, comparison of the laser-excited fluorescence spectra and lifetime of Nd^{3+} with the corresponding results from pure oxide and fluoride glasses demonstrates the presence of Nd^{3+} sites having both fluorine and oxygen nearest-neighbor coordination.

INTRODUCTION

Until recently, spectroscopic characterization of the fluorescent properties of glasses has always been restricted to values averaged over the randomly disordered environment characteristic of the host matrix. The development of laser-induced fluorescence line narrowing[1,2] (FLN), however, has made it possible to overcome some of the limitations that this inhomogeneous broadening imposes on the understanding of such systems. In this technique a short laser pulse of narrow spectral width is used to excite an energetically specified subset of ionic environments within the inhomogeneously broadened absorption profile. The emission from this subset is measured by gated detection before substantial cross relaxation can take place between ions in different sites, resulting in an emission spectrum characteristic of only that subset of ions originally excited. By exciting at a sequence of different wavelengths within an inhomogeneously broadened absorption line, the full range of microscopic environments are probed and the site-dependent behavior of all the spectroscopic properties of the ion-host medium are explored.

Previous studies of fluorescence line narrowing in glass have treated ion-ion energy transfer in inhomogeneously broadened systems,[3,4] variations in the coordination structure of rare-earth ions in various oxide[5,6] and fluoride[7] glasses, and homogeneous linewidth studies.[8,9] Recent experiments have revealed large site-dependent variations of the radiative and nonradiative transition probabilities and quantum efficiencies of paramagnetic ions in glass,[10,11] and a particular study was made of the kinetics of trivalent neodymium ions in a silicate laser glass, ED-2.[10] In this paper we extend the fluorescence line narrowing and kinetic studies of Nd^{3+} to a series of widely differing oxide and fluoride glasses. Various spectroscopic parameters are characterized, and their similarities and differences rationalized with respect to the individual properties of the glass matrices.

EXPERIMENTAL

Neodymium ions were excited via their $^4I_{9/2} \rightarrow {}^2P_{1/2}$ absorption. This transition was selected because of its spectral simplicity: First, at sufficiently low (liquid-helium) temperature, only the lowest Stark level of the ground $^4I_{9/2}$ multiplet is populated; and, second, the upper level is a single isolated Kramers-degenerate state. Consequently, the total linewidth is unaffected by Stark splitting, and arises virtually entirely from site-to-site variations in the environment of the emitting ions. Excitation into the $^2P_{1/2}$ state is followed by a rapid (<50 nsec) level-by-level nonradiative cascade to the $^4F_{3/2}$ state.[12] At low temperatures, the population is restricted to the lowest Stark level of $^4F_{3/2}$, from which fluorescence is observed.

A tunable pulsed dye laser was used for the line-narrowing and kinetics studies. The laser consisted of an alcoholic solution of Coumarin 120 dye circulated through a cylindrical cell with wedged windows and excited transversely by an Avco C950

pulsed nitrogen laser. The dye-laser pulses were ≈15 nsec in duration with a spectral width <0.1 nm. The laser wavelength was tuned over a 10-nm range centered around 430 nm by an intracavity grating.

The emission from the samples, maintained in a liquid helium cryostate at about 10 K, was measured with a Jarrell-Ash 1-m Czerny-Turner spectrometer and a Varian VPM-159S photomultiplier. The relatively flat detector response out to 1.1-μm minimized variations in spectral sensitivity and permitted precise calibration of the emission intensity. A PAR Model 160 boxcar integrator provided time-resolved integration of the fluorescence signal.

Five glass specimens were examined; their identities and material parameters are given in Table I. The emission spectra were generally measured with a gate width of 50 μsec at a delay of 100 μsec after the excitation pulse. This delay time was long enough to suppress transient rise-time effects, and short enough to minimize cross-relaxation to the remainder of the ensemble of ions. (For the faster-relaxing borate sample, a 20-μsec gate and a 50-μsec delay were used.) Pulse repetition rates were less than 50 sec^{-1}. The spectra were recorded in the 0.85–0.95 and 1.0–1.1-μm regions, corresponding to $^4F_{3/2} \rightarrow {}^4F_{9/2}$ and $^4F_{3/2} \rightarrow {}^4I_{11/2}$ transition, and normalized in terms of photons emitted per constant number of excitation photons actually absorbed by the specimen. This normalization required measurement of both the absorption coefficient and the laser power at each excitation wavelength. The absorption profile was also measured in the 0.88-μm region, where resonance self-absorption can be large enough to distort the shape of the emission spectrum. Correction for this distortion can be readily calculated and the effect minimized; however, at liquid-helium temperatures, where the distortion is limited to the shortest wavelength component of the $^4F_{3/2} \rightarrow {}^4I_{9/2}$ transition, the effect on the total emission is inconsequential.

RESULTS

The $^4I_{9/2} \rightarrow {}^2P_{1/2}$ absorption profiles for the five glasses at liquid-He temperature are shown in Fig. 1. The dye laser was tuned at 0.5-nm intervals across these absorption bands and the fluorescence recorded. The resulting line-narrowed $^4F_{3/2} \rightarrow {}^4I_{9/2}$ and $^4F_{3/2} \rightarrow {}^4I_{11/2}$ spectra, corrected for detector response and normalized to a constant number of absorbed photons, are shown in Figs 2–6.

TABLE I. Chemical composition and properties of host glasses.

GLASS TYPE	HOST COMPOSITION (mol %)		Nd^{3+} DOPANT ION DENSITY (10^{20} ions/cm^3)	HOST DENSITY (g/cm^3)	REFRACTIVE INDEX n_D	$n(n^2+2)^2$
Silicate	SiO_2	60	0.927	2.54	1.5716	31.40
	Li_2O	27.5				
	CaO	10				
	Al_2O_3	2.5				
Phosphate	P_2O_5	50	0.971	2.78	1.5162	28.02
	K_2O	33.3				
	BaO	16.7				
Borate	B_2O_3	67	0.86	3.08	1.5826	32.11
	BaO	18				
	Na_2O	15				
Fluoroberyllate	BeF_2	49	2.62	2.58	1.3445	19.49
	KF	27				
	CaF_2	14				
	AlF_3	10				
Fluorophosphate	AlF_3	40	1.88	3.55	1.4438	24.09
	CaF_2	30				
	MgF_2	10				
	SrF_2	10				
	BaF_2	5				
	$Ba(PO_3)_2$	5				

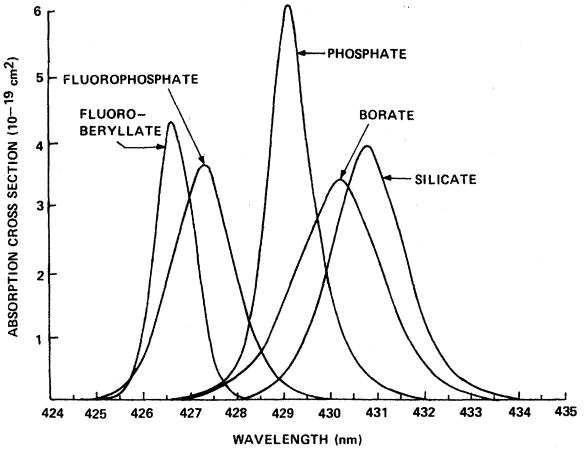

FIG. 1. Absorption cross sections of the inhomogeneously broadened $^4I_{9/2} \rightarrow {}^2P_{1/2}$ transition of Nd^{3+} in the various glasses at liquid-helium temperature.

The total intensities in the two spectral bands were measured by graphical integration. The ratio of these intensities as a function of excitation wavelength is plotted in Fig. 7.

The Nd^{3+} fluorescence decay was also measured at each excitation wavelength. In constrast to the behavior under nonselective broadband excitation, where initial and later e-folding times are observed to differ by more than 50% in some silicate glasses, the laser-excited decays were definitively characterized by single-exponential time dependences. The lifetimes for the various glasses obtained from a least-squares fit of the decay are shown in Figs. 8(a)–12(a), again as a function of excitation wavelength.

The total time-integrated fluorescence intensities were calculated from the lifetimes and the time-resolved integrated intensities. The resulting values are proportional to the ratio of total emitted photons to total absorbed photons, and are a measure of the quantum efficiency. The variations in the relative quantum efficiencies with excitation wavelength are also shown in Figs. 8(b)–12(b). In these plots the highest relative quantum efficiency is normalized to unity for four of the glasses, since, as discussed later, either direct measurements or indirect determinations of the absolute quantum efficiencies indicate that this assumption is a reasonable approximation. For the borate glass the quantum efficiency is known to be much less than unity and is scaled to the estimated overall value. By combining the excitation wavelength dependences of the total lifetime and the radiative intensity, the site-to-site variations of both the radiative and nonradiative decay rates are obtained. These rates as a function of excitation wavelength are shown in Figs. 8(c)–12(c).

Estimates of the average radiative transition probabilities for the various glasses were made using the Judd-Ofelt treatment of rare-earth spectral intensities. This approach has been applied previously to f-f transitions of Nd^{3+},[13,14] and other rare earths[15] in glasses. The line strength of a

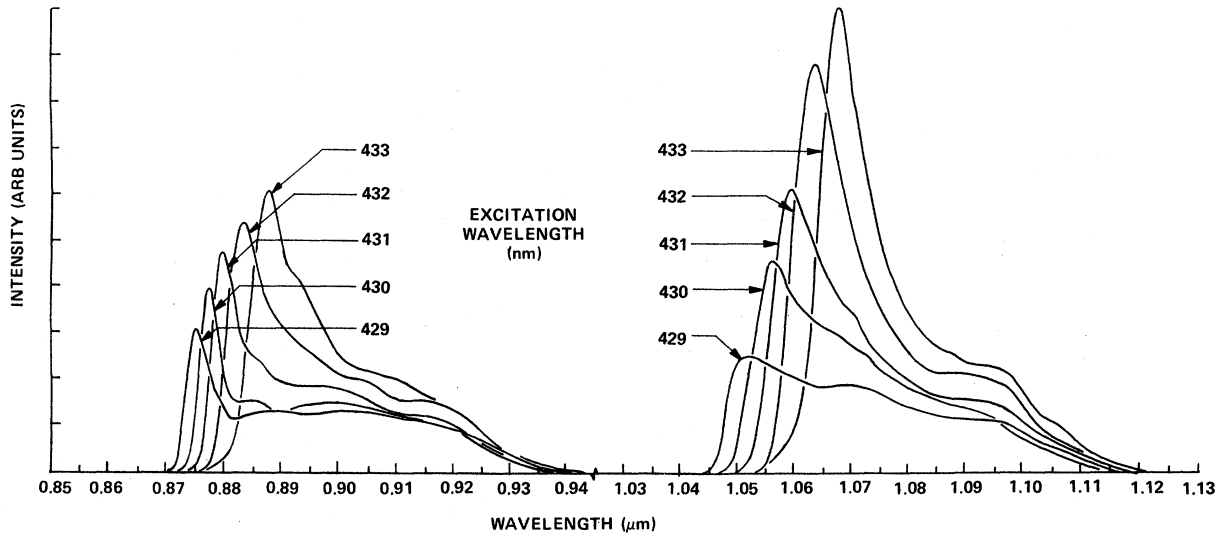

FIG. 2. Line-narrowed fluorescence spectra of Nd^{3+} in silicate glass as a function of excitation wavelength. In this and subsequent figures, the intensities (at liquid-helium temperature) are given in terms of photons emitted for equal numbers of excitation photons absorbed and are normalized to the highest emission peak as unity. The fluorescence was measured 100 μsec after the excitation pulse; the spectra are not normalized for differences in decay times.

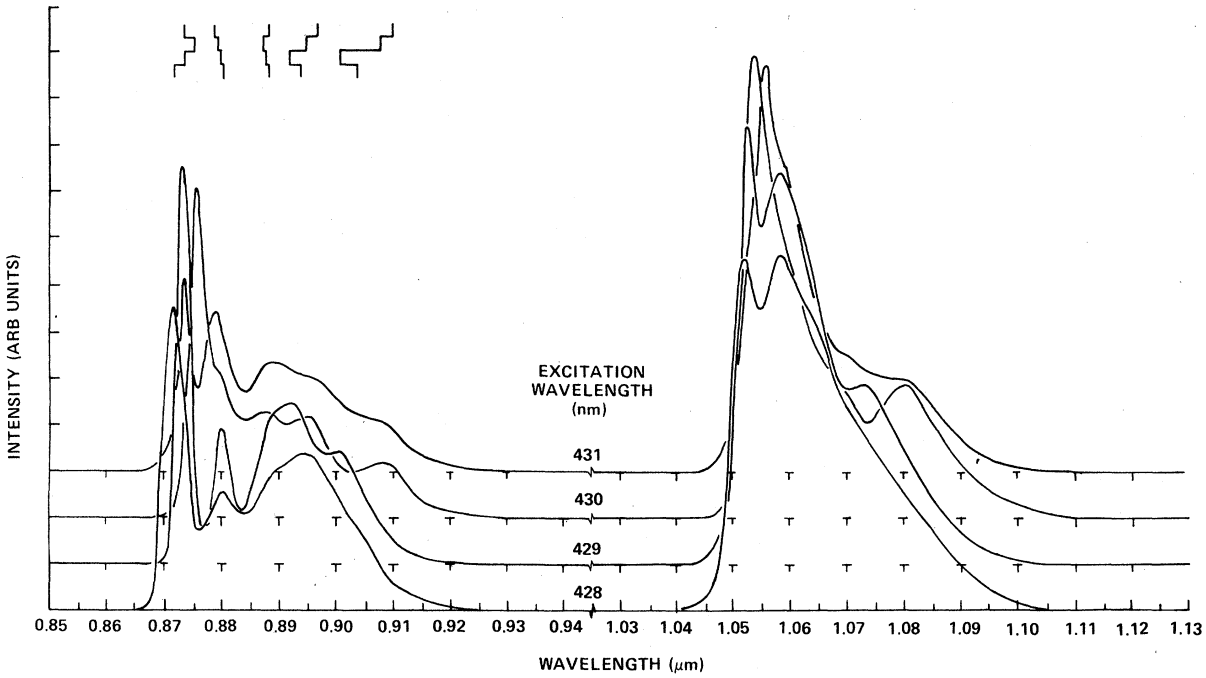

FIG. 3. Line-narrowed fluorescence spectra of Nd^{3+} in phosphate glass as a function of excitation wavelength. Conditions are the same as in Figs. 2 and 3.

transition between two J states is given by

$$S(J;J') = \sum \Omega_t \left| \langle (\alpha SL)J \| U^{(t)} \| (\alpha' S' L')J' \rangle \right|^2 , \quad t = 2, 4, 6 , \quad (1)$$

where the coefficients Ω_2, Ω_4, and Ω_6 are phenomenological intensity parameters, and the $\langle \| U^{(t)} \| \rangle$ terms are doubly reduced matrix elements of unit tensor operators. The values of Ω_2, Ω_4, and Ω_6 were determined by a least-squares fit of Nd^{3+} absorption bands in the 400–900-nm region, and are given in Table II. The experimental error is associated with the quality of the fit and does not include uncertainties in the Nd concen-

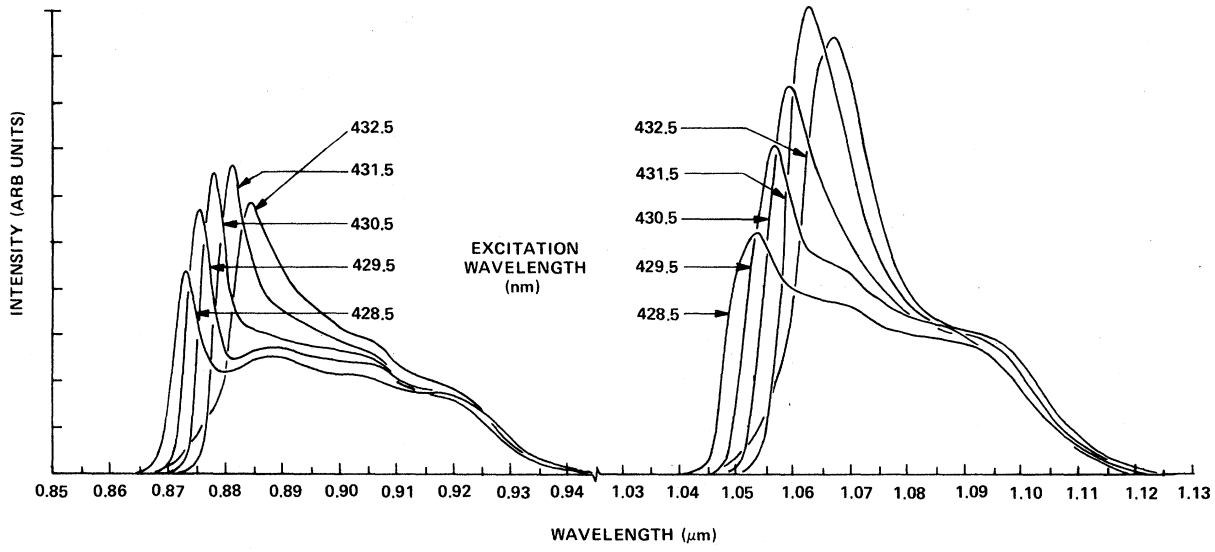

FIG. 4. Line-narrowed fluorescence spectra of Nd^{3+} in borate glass as a function of excitation wavelength. Conditions are the same as in Fig. 2, except that the delay between excitation and measurement was reduced to 50 μsec.

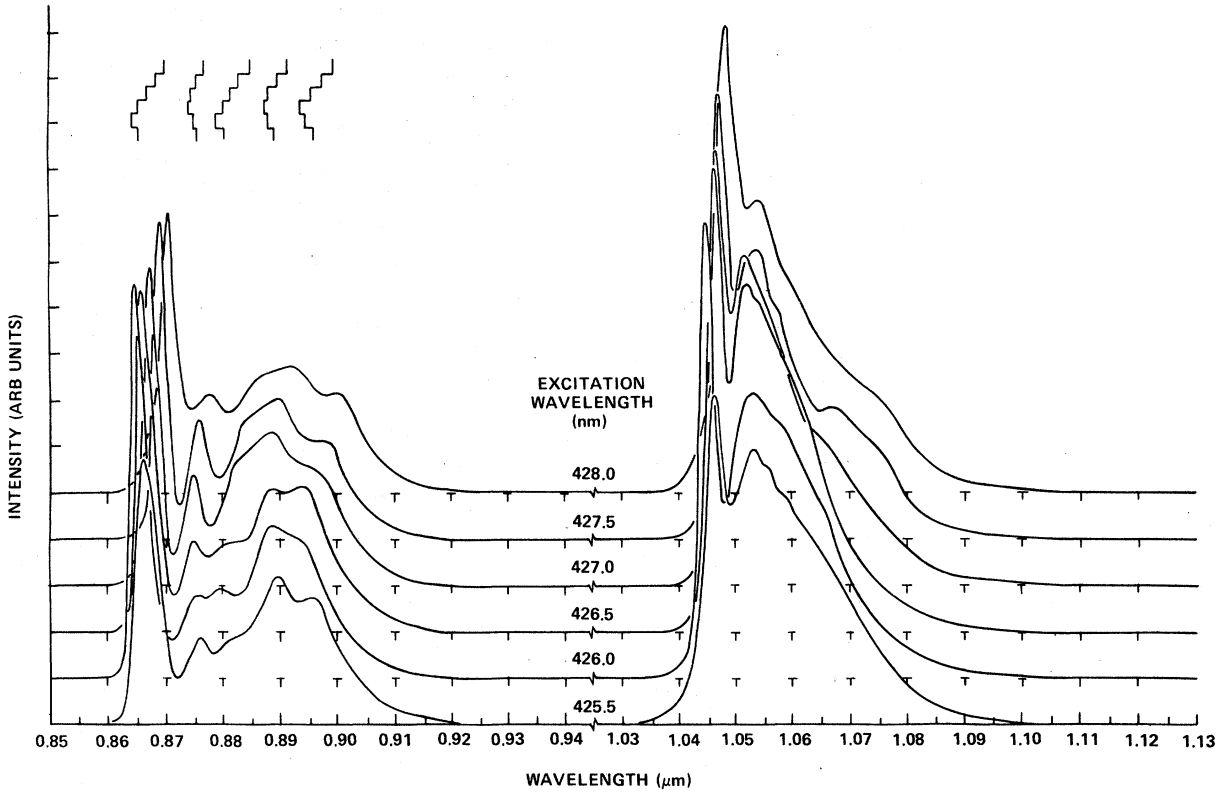

FIG. 5. Line-narrowed fluorescence spectra of Nd^{3+} in fluoroberyllate glass as a function of excitation wavelength. Conditions are the same as in Fig. 2, but the spectra are displayed with a vertical offset to increase clarity. The stroke marks above the spectra indicate the excitation-dependent wavelengths of the five components of the $^4F_{3/2} \rightarrow {}^4I_{9/2}$ transition.

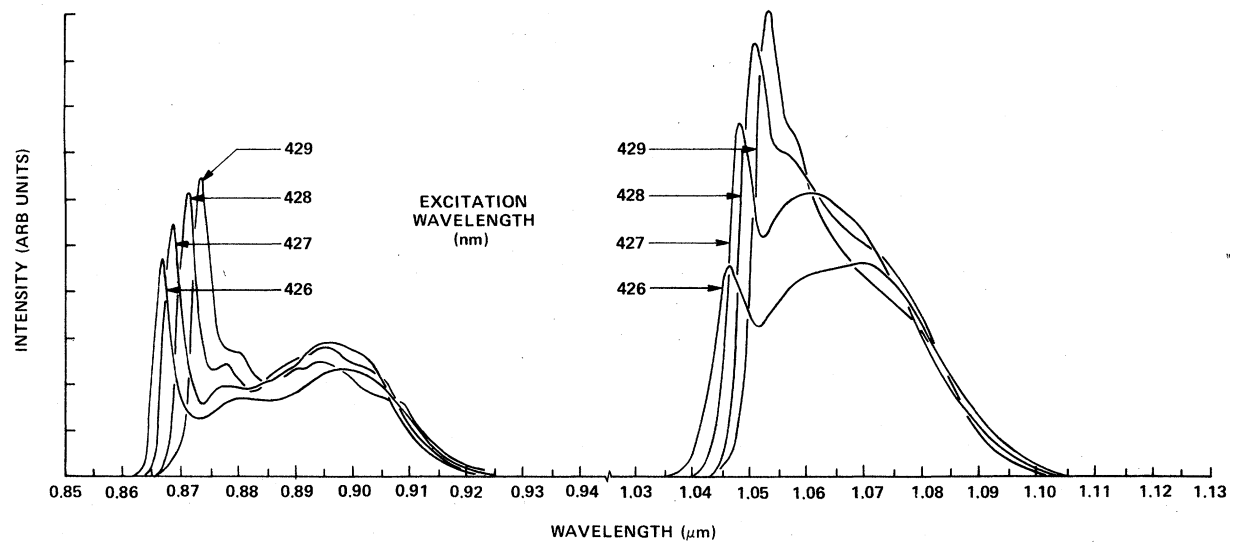

FIG. 6. Line-narrowed fluorescence spectra of Nd^{3+} in fluorophosphate glass as a function of excitation wavelength. Conditions are the same as in Figs. 2 and 3.

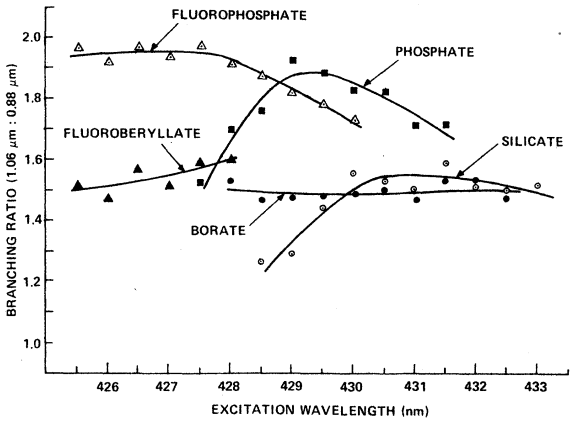

FIG. 7. Ratios of the total emission (integrated over wavelength and time) in the $^4F_{3/2} \rightarrow {}^4I_{11/2}$ transition to the corresponding total in the $^4F_{3/2} \rightarrow {}^4D_{9/2}$ transition for Nd^{3+} in various glasses.

tration or measurement procedures. For a particular ion-host combination, the Ω values are then used to calculate the line strength of transitions between any $4f$ states of interest. In the case of the $^4F_{3/2}$ state, the spontaneous emission probabilities to all levels of the ^4I ground multiplet were calculated from the expression

$$A(^4F_{3/2}; {}^4I_{J'}) = \frac{64\pi^4 e^2}{3h(2J+1)\bar{\lambda}^3} \frac{n(n^2+2)^2}{9} \times \sum_t \Omega_t |\langle (\alpha SL)J || U^{(t)} || (\alpha' S' L')J' \rangle|^2 . \quad (2)$$

Here $\bar{\lambda}$ is the average wavelength of the transition and n is the refractive index at this wavelength as computed from the sodium D-line index in Table I and the dispersion (Abbe number). The radiative

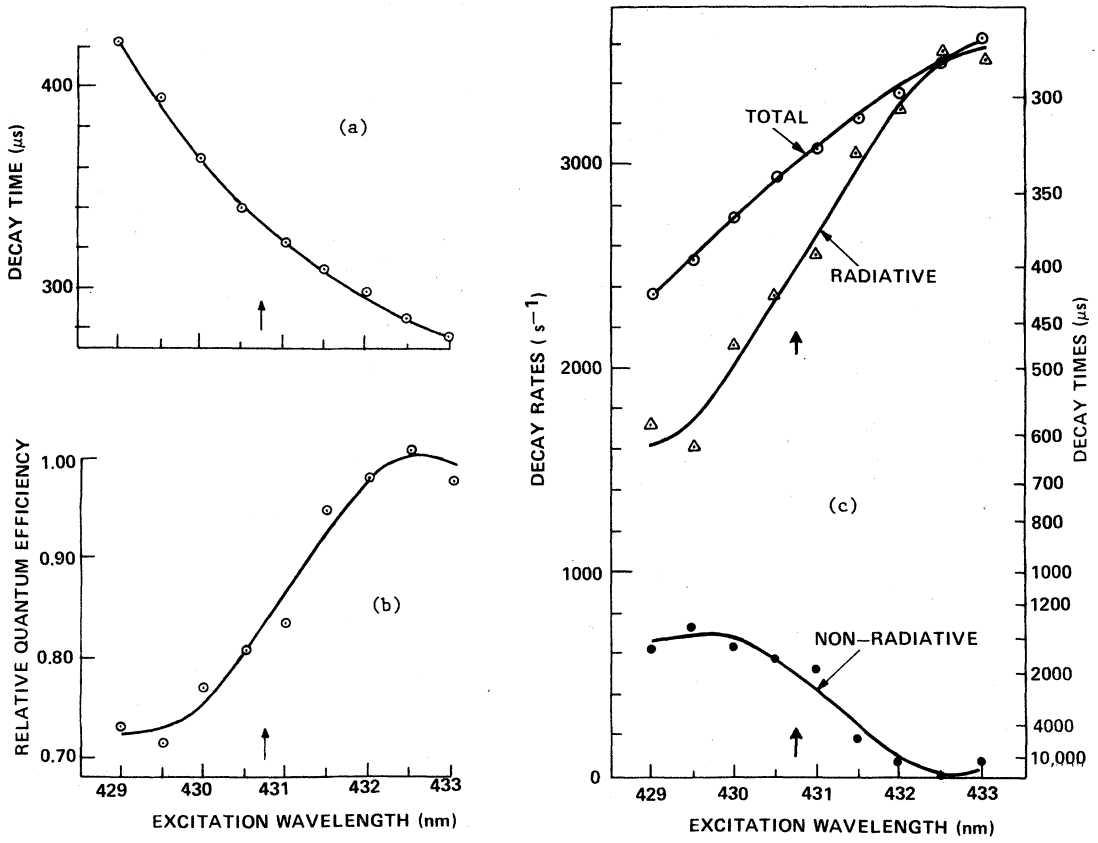

FIG. 8. Excitation wavelength dependence of (a) the fluorescence decay time, (b) the relative quantum efficiency, and (c) the radiative and nonradiative decay rates of Nd^{3+} in the silicate glass. The wavelength of the excitation peak is indicated by an arrow. The relative quantum efficiency is taken as the sum of the total emission (integrated over wavelength and time) in the $^4F_{3/2} \rightarrow {}^4I_{9/2}$ and $^4F_{3/2} \rightarrow {}^4I_{11/2}$ transitions, normalized to the maximum value as unity. The radiative and nonradiative rates were calculated from the total (measured) rate and the relative quantum efficiency, as discussed in the text.

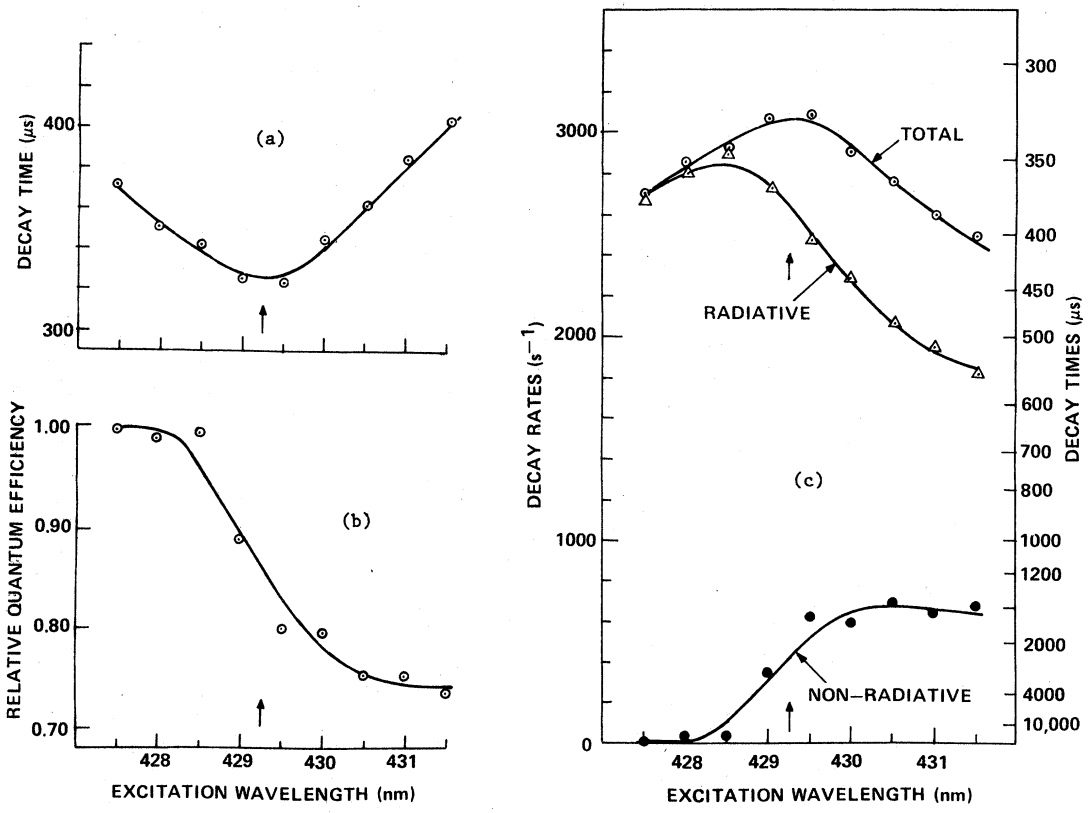

FIG. 9. Excitation wavelength dependence of (a) the fluorescence decay time, (b) the relative quantum efficiency, and (c) the radiative and nonradiative decay rates of Nd^{3+} in the borate glass. Conditions as in Fig. 8, except that in this case the relative quantum efficiency has been scaled to reflect the true overall quantum efficiency of about 15%.

lifetime of the $^4F_{3/2}$ state was obtained from

$$\tau_R^{-1} = \sum A(^4F_{3/2}; {}^4I_{J'}), \tag{3}$$

where the summation is over all $^4I_{J'}$ terminal states; these results are tabulated in Table II. The radiative branching ratio is given by

$$\beta(^4F_{3/2}; {}^4I_{J'}) = A(^4F_{3/2}; {}^4I_{J'}) \Big/ \sum_J A(^4F_{3/2}; {}^4I_J), \tag{4}$$

and is also included in Table II. The only emission of consequence not measured directly is that of the $^4F_{3/2} \rightarrow {}^4I_{13/2}$ transition at ≈ 1.3–1.4 μm, which was beyond the range of our detector. As shown elsewhere,[14] the branching ratio to $^4I_{13/2}$ never exceeds ~0.15, and is typically 0.1 ± 0.01 for the present glasses. Because of the relatively small size and even smaller variation of this contribution, only a small error is introduced by treating it as a constant. The branching ratio to $^4I_{15/2}$ is less than 0.01 and is negligible compared to experimental uncertainties.

DISCUSSION

The five glasses that were studied exhibit a diversity of behavior, both in the crystal-field splitting shown by the line-narrowed fluorescence and in the site dependence of the radiative and nonradiative transition probabilities. Among the various glass types, the differences are more striking than the similarities; we shall therefore discuss each glass separately before attempting to generalize.

Silicate glass

The present results are an extension of previously reported data on ED-2 glass.[10] The line-narrowed fluorescence in Fig. 2 shows only broad and poorly defined spectral features. None of the five components of the $^4F_{3/2} \rightarrow {}^4I_{9/2}$ transition nor any of the six components of the $^4F_{3/2} \rightarrow {}^2I_{11/2}$ transition could be followed through the series of excitation wavelengths with any degree of confidence.

The fluorescence decay time in Fig. 8(a) decreases smoothly and monotonically from over 400 μsec at short excitation wavelengths to below 300

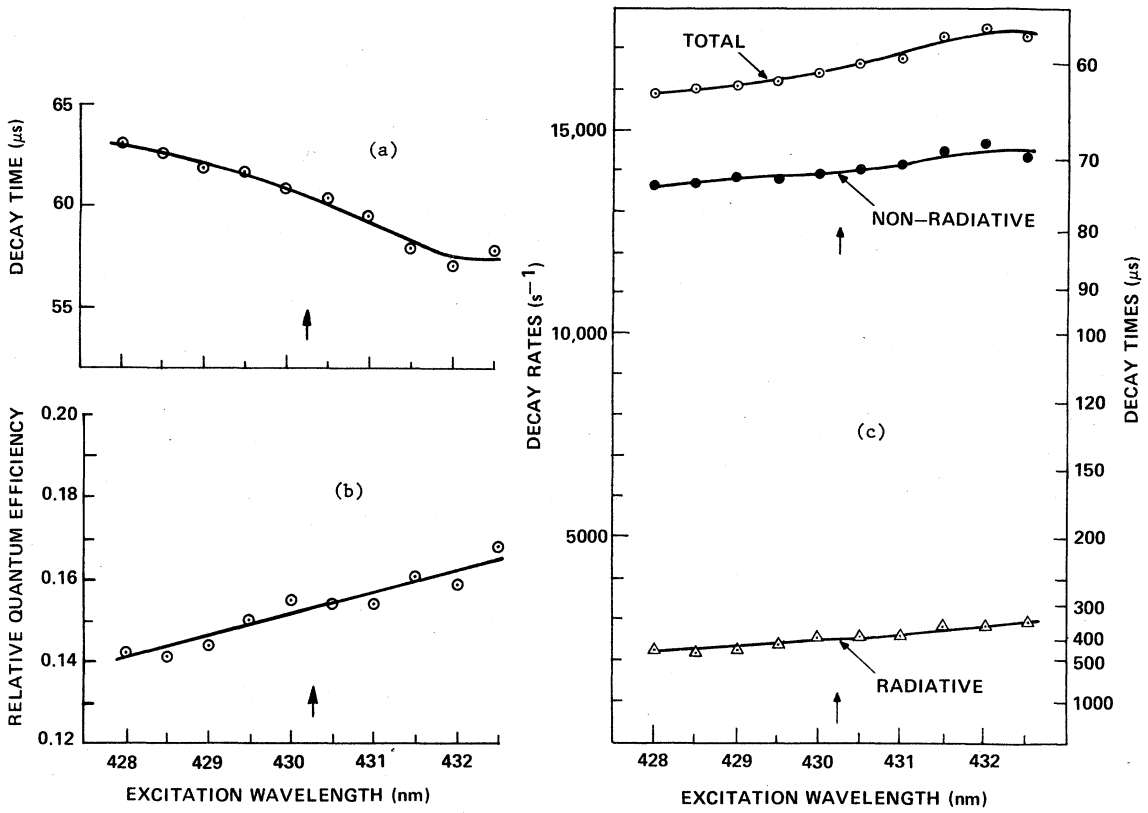

FIG. 10. Excitation wavelength dependence of (a) the fluorescence decay time, (b) the relative quantum efficiency, and (c) the radiative and nonradiative decay rates of Nd^{3+} in the phosphate glass. Conditions as in Fig. 8.

μsec at the long-wavelength extreme; the relative quantum efficiency increases by one-third over the same range. Based upon the normalization to unit quantum efficiency in Fig. 8(b), the radiative decay *rate* in Fig. 8(c) is seen to change by a factor of 2 while the nonradiative decay rate increases from zero to a maximum rate of about 7×10^2 sec^{-1}. The average nonradiative decay rate of $\approx 5\times 10^2$ sec^{-1} is consistent with the rates derived from spectroscopic determination and absolute measurements of the quantum efficiency[16] and from extrapolation of multiphonon relaxation rates for the $^4F_{3/2}\rightarrow{}^4I_{15/2}$ energy gap of Nd^{3+}.[17]

Phosphate glass

The fluorescence spectra of this glass (Fig. 3) are less extended and show more structure than in the case of the silicate glass. All five components of the $^4F_{3/2}\rightarrow{}^4I_{9/2}$ transition are resolvable, and can be followed through the series of different excitation wavelengths. The changing pattern of crystal-field splittings of the $^4I_{9/2}$ manifold is shown above the spectra.

The behavior of the fluorescence decay time, in contrast to that of the silicate glass results, is not monotonic. As shown in Fig 9(a), it initially decreases by ≈20%, reaches a minimum at about the middle of the excitation range, then increases more than 25% at longer wavelengths. The relative quantum efficiency, however [Fig. 9(b)], increases monotonically in a sigmoidal fashion over the same range. This indicates that two competing effects are active: a decreasing radiative rate opposed by an increasing nonradiative rate. These rates are plotted in Fig. 9(c). The average value for the nonradiative decay rate is about the same as for the silicate glass, while the average quantum efficiency is fractionally higher.

Borate glass

The borate glass spectra in Fig. 4 are similar to those of the silicate glass in both breadth and structural detail. However, other spectroscopic properties of the borate glass are unique. It is the only one of the glasses whose average quantum efficiency is substantially less than unity; conse-

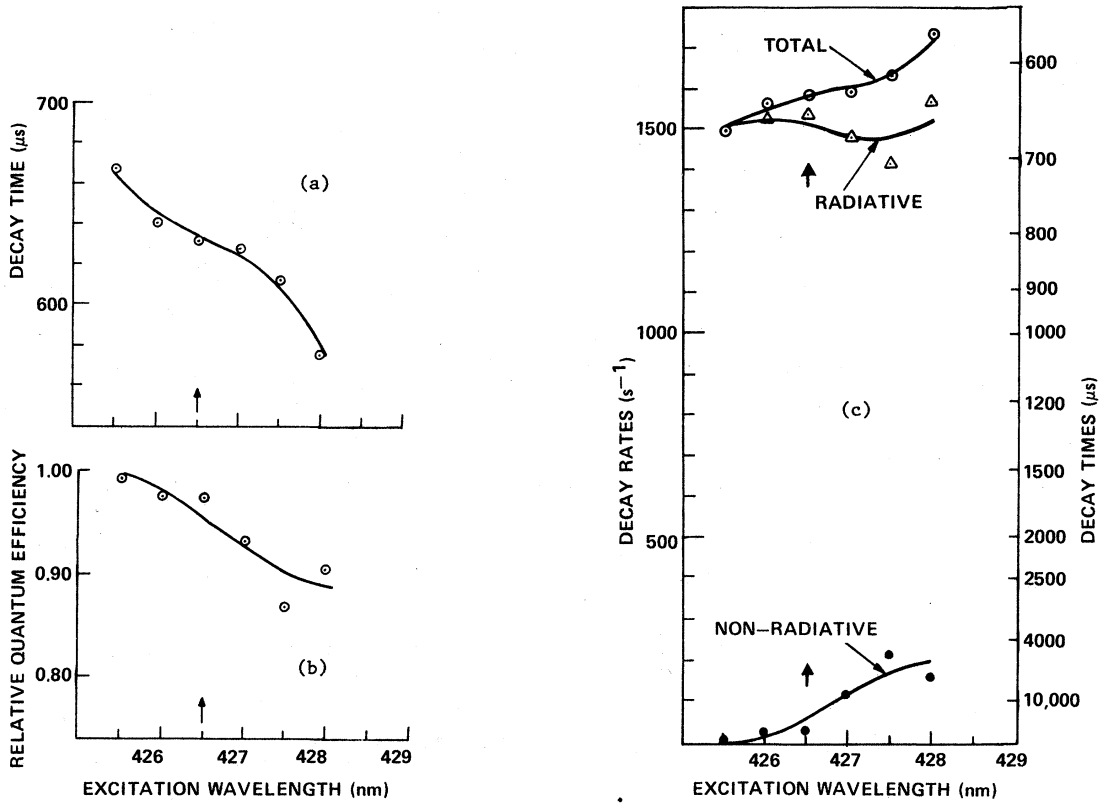

FIG. 11. Excitation wavelength dependence of (a) the fluorescence decay time, (b) the relative quantum efficiency, and (c) the radiative and nonradiative decay rates of Nd^{3+} in the fluoroberyllate glass. Conditions as in Fig. 8.

quently, its fluorescence decay time is much shorter than in the other glasses. The fluorescence lifetime decreases monotonically and the relative quantum efficiency simultaneously increases by about 15% over the excitation range, as shown in Figs. 10(a) and 10(b). Thus, the nonradiative rate is not only large but shows only a small variation over the entire range [see Fig. 10(c)], consistent with the reasonably exponential decay observed under broad band excitation. If the nonradiative rate is assumed to be constant, the best nonlinear least-squares fit to the data gives a value of $\approx 1.4 \times 10^4$ sec^{-1} and an average quantum efficiency of ≈16%.

The small site-to-site variation in the nonradiative decay rate exhibited by this borate glass is relatively unusual. Other studies of nonradiative decay in glasses by multiphonon emission show that large variations in decay rates are possible[11]; for example, a nonradiative variation of ≈2.5 was observed for Er^{3+} in fluoroberyllate glass.[18] The differences are confirmed by measurements of the $^3F_4 \rightarrow {}^3H_5$ multiphonon decay of Tm^{3+} in the present borate glass composition and in a silicate and a phosphate glass.[12] The decay from the borate glass through the fourth e-folding times fit a single exponential time dependence. In contrast, in the silicate and phosphate glasses, where the relaxation was again dominated by multiphonon emission, the first and fourth e-folding times ranged ≈30–75 and 30–60 μsec, respectively.[19] Therefore, the uniformity of the nonradiative decay rates with site appears to be a unique characteristic of this particular borate glass

Fluoroberyllate glass

The results for this material represent an opposite extreme of behavior. The line-narrowed fluorescence (Fig. 5) shows well-resolved features, and all five of the $^4F_{3/2} \rightarrow {}^4I_{9/2}$ components can be followed across the entire excitation range. Even in the $^4F_{3/2} \rightarrow {}^4I_{11/2}$ region, where the spectral features are not as well defined, most of the six components can be located with reasonable confidence. The comparatively low degree of inhomogeneous broadening (also seen in the narrowness of the excitation line) indicates a glass with small site-to-site variations in the local field. Attempts to model the variations in the local structure and

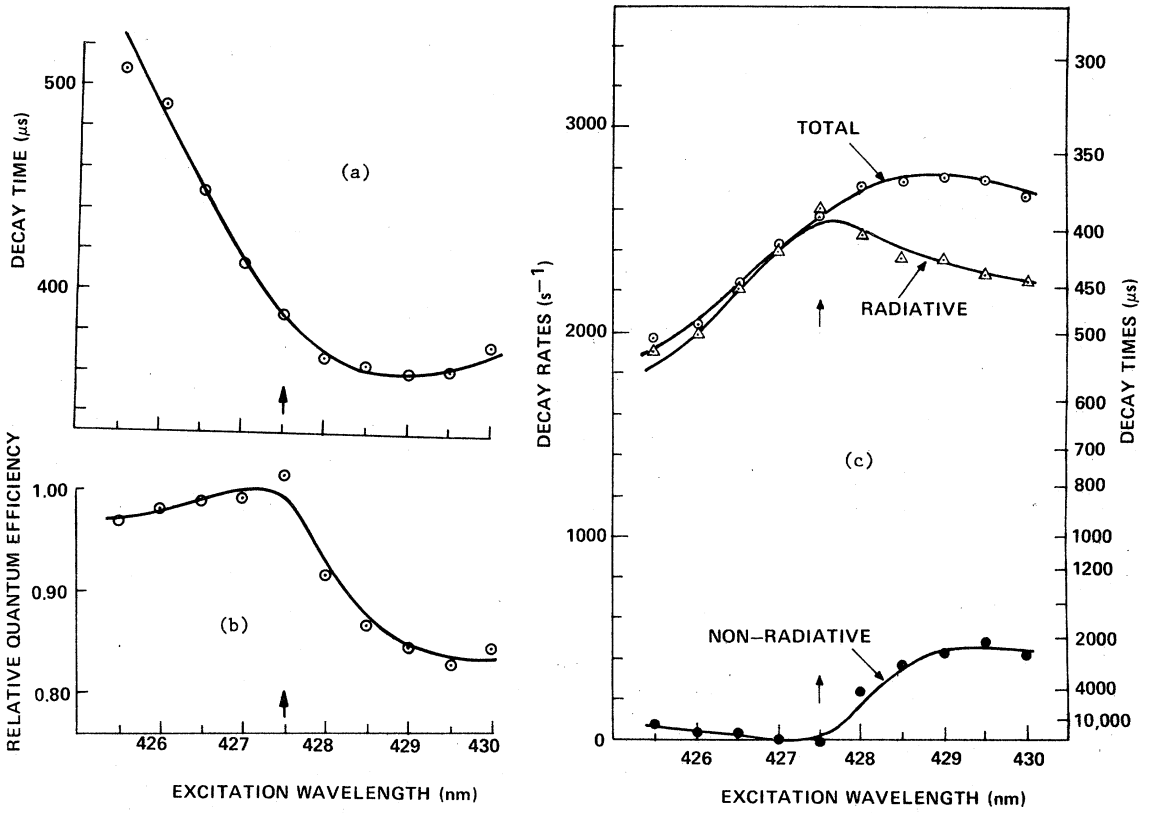

FIG. 12. Excitation wavelength dependence of (a) the fluorescence decay time, (b) the relative quantum efficiency, and (c) the radiative and nonradiative decay rates of Nd^{3+} in the fluorophosphate glass. Conditions as in Fig. 8.

coordination using crystal-field parameters derived from the above spectra are in progress.[7]

The fluorescence decay time and the relative quantum efficiency both decrease montonically with increasing excitation wavelength, but by only about 10% [Figs. 11(a) and 11(b)], which is not much greater than the scatter of the intensity measurements. This indicates an almost constant radiative decay rate, accompanied by a small nonradiative rate [Figs. 11(c)]. An average nonradiative rate of $\approx 10^2$ sec^{-1} is in agreement with extrapolated rare-earth multiphonon emission rates.[18]

Fluorophosphate glass

The fluorophosphate glass exhibits a strange combination of properties. In some ways, such as the wavelengths of absorption and emission (Figs.

TABLE II. Judd-Ofelt intensity parameters and calculated radiative lifetimes and branching ratios for the $^4F_{3/2}$ state of Nd^{3+} in glasses at 295 °K.

GLASS TYPE	INTENSITY PARAMETERS (10^{-20} cm^2)			RADIATIVE LIFETIME (μsec)	BRANCHING RATIOS		
	Ω_2	Ω_4	Ω_6		β(9/2)	β(11/2)	β(11/2)/β(9/2)
Silicate	3.23 ± 0.12	4.59 ± 0.28	4.80 ± 0.13	359	0.421	0.484	1.15
Phosphate	3.34 ± 0.24	4.98 ± 0.35	5.63 ± 0.16	353	0.406	0.496	1.22
Borate	4.37 ± 0.22	3.59 ± 0.32	4.68 ± 0.14	394	0.388	0.507	1.31
Fluoroberyllate	0.23 ± 0.27	3.92 ± 0.40	4.60 ± 0.12	613	0.396	0.505	1.28
Fluorophosphate	1.86 ± 0.28	4.13 ± 0.41	5.02 ± 0.18	465	0.392	0.507	1.29

1 and 6), the spectroscopic properties fall intermediate between the pure phosphate and fully fluorinated fluoroberyllate. However, the structural detail of the spectra are quite unlike either, with a larger Stark splitting of the components and a far greater inhomogeneous broadening.

The fluorescence decay time in Fig. 12(a) shows the greatest variation seen in any of the glasses, dropping precipitously by more than 30% as the excitation wavelength is increased from the short wavelength limit, then leveling off to an essentially constant value at the longer wavelengths. The relative quantum efficiency [Fig. 12(b)] remains nearly constant for excitation wavelengths shorter than midrange, but drops off by about 15% at longer wavelengths. This complex behavior is also reflected in the resulting radiative and nonradiative decay rates [Fig. 12(c)], and is discussed in more detail later.

Fluorescence linewidths, wavelengths, and transition probabilities

None of the laser-excited fluorescence spectra in Figs. 2–6 show the extreme line narrowing expected for resonant excitation and observation.[8] Instead, transitions between Stark levels exhibit linewidths much broader than the homogeneous widths. This is attributed to a residual inhomogeneous broadening, which occurs for nonresonant fluorescence, because the excitation energy of ions in physically distinct sites may accidentally coincide while the locations of other levels remain different.[20] Another manifestation of such accidental coincidence is the occurrence of nonexponential fluorescence decays following pulsed narrowband excitation; although this has been observed under other circumstances,[5] the approximately exponential decays here indicate that this variation is small for the present experiments.

The centers of gravity of the $^4I_{9/2} \rightarrow {}^2P_{1/2}$ absorption spectra and the $^4F_{3/2} \rightarrow {}^4I_{9/2}$ and $^4F_{3/2} \rightarrow {}^4I_{11/2}$ fluorescence spectra occur at different wavelengths for the various glasses. This is due to the nephelauxetic effect, where because of the large Nd^{3+} nearest-neighbor anion interaction, the Racah parameters and the separation of the free-ion states are reduced. Thus because of the greater covalency of the oxide glasses, their spectra are shifted to longer wavelengths.

The radiative lifetimes in Table II are calculated from intensity parametes derived from absorption spectra that sum contributions from ions in sites having different number densities, thermal level populations, and line strengths. Therefore the calculated lifetime should represent some averaged lifetime rather than the extremes. This is the case for all glasses studied; the calculated lifetime values in Table II fall between the longest and shortest values measured under FLN conditions.

The fluorescence branching ratios β in Table II again represent some effective average over the different sites. The ratios of the branching ratios to $^4I_{11/2}$ and $^4I_{9/2}$ in Table II are smaller than any of the measured values in Fig. 7. Studies of a large number of different glasses[14] have shown that the line strength of the $^4I_{9/2} \rightarrow {}^4F_{3/2}$ transition of Nd^{3+} calculated from Judd-Ofelt parameters is usually larger than the observed value by up to ≈15%. The probability for the related radiative transition $^4F_{3/2} \rightarrow {}^4I_{9/2}$ is, therefore, also expected to be too large. In the absence of other or compensating discrepancies for the other $^4F_{3/2} \rightarrow {}^4I_{11/2}$ transitions (which are, at present, unknown), this will reduce the $\beta(\frac{11}{2})/\beta(\frac{9}{2})$ ratio in Table II from its true value. Although the absolute magnitudes are not in quantitative agreement with experiment, the predicted trend is generally correct.

Comparison of line-narrowed fluorescence spectra

The patterns of the laser-excited fluorescence spectra for the five glasses studied can be grouped into three broad categories. The first consists of the silicate and borate glasses, which have large Stark splittings and a relatively low degree of local order. These glasses are characterized by laser-excited fluorescence bands having poorly resolved components and a large residue of inhomogeneous broadening. Because of the nephelauxetic effect, their emission and absorption bands occur at longer wavelengths than those of the other glasses.

These two glasses also show similar site-dependent behavior of their relative quantum efficiency and radiative decay rates. The only substantive difference is in the nonradiative decay rate, and hence the absolute quantum efficiency. In the silicate the relative nonradiative rate change is large; in the borate roughly the same range of variation in absolute terms amounts to only about 10% of the total. The small site dependence of the multiphonon decay rate could be attributed to a reduced-mass effect: the oxygen (in the first coordination sphere of the Nd^{3+} ion) accounts for almost two-thirds of the total motion in a Si-O-Nd vibration but only about one-third of the total in a B-O-Nd vibration. Since the effects of ions beyond the first coordination sphere (for example, boron) are likely to be representative of the average behavior in the bulk matrix rather than a localized site, it should not be surprising to find a smaller site dependence of phonon-dependent processes in the latter case.

The phosphate and fluoroberyllate glasses fall into a second category. Both glasses have a higher degree of order, as indicated by the greater resolution of these spectral components and smaller residual inhomogeneous broadening. Although this is not as true for the phosphate as for the fluoroberyllate, their spectra resemble each other far more than those of the silicate or borate. The extent of the Stark splittings of the $^4I_{9/2}$ and $^4I_{11/2}$ manifolds is not as great in the fluoride as in the oxide glass. Also, the probabilities for radiative and nonradiative transitions are smaller in the fluoroberyllate than in the phosphate. These two results are typical for totally fluorine-based rather than oxygen-based hosts. Both of the glasses show a similar site dependence of their relative quantum efficiency.

Finally, the third and most interesting category of glasses is the fluorophosphate, the only mixed anion glass studied. As stated earlier, some characteristics, such as the wavelengths of emission and absorption, fall between those of the phosphate and fluoroberyllate. More important, however, are those characteristics exhibiting a dichotomy. For excitations shorter than midrange the site-dependent behavior of the fluorophosphate becomes progressively more like that of the fluoroberyllate; the quantum efficiency is near unity, while the overall decay time becomes much longer than is observed in any oxide system. For excitations at wavelengths longer than midrange, the behavior of both quantum efficiency and decay time are similar to those of the phosphate. The similarity in radiative decay rates is even more striking if one applies the local-field correction to the spontaneous emission probability, which enters in the form of $n(n^2+2)^2$. Using the known values for the index of refraction (Table I), we find that a radiative decay rate of 2×10^3 per second, typical of sites near the short-wavelength excitation limit of the fluorophosphate, would be reduced to a value of 1.62×10^3 in the fluoroberyllate; similarly, a radiative decay rate of 2.2×10^3, typical of sites near the long-wavelength excitation limit of the fluorophosphate, corresponds to a value of 2.56×10^3 in the phosphate. Both extremes are in good agreement with values actually found in the glasses. On the basis of these points, we propose that the fluorophosphate contains a range of sites in which, over the commonly found geometrical changes of coordination, an even greater change—the coordinating species itself—is superimposed. Thus at the shorter-wavelength excitations of the fluorophosphate we are observing emissions from Nd^{3+} ions largely coordinated with fluoride, while at the longer-wavelength excitations emission from largely oxide-coordinated sites becomes dominant. This accounts for the poor resolution and apparently large inhomogeneous width of the fluorophosphate spectra; even if the sites were reasonably well ordered geometrically, they would be chemically distinct.

In this context, it is interesting to note that not even at the extremes of the excitation range does the fluorophosphate spectrum become sharp enough to resemble those of either the pure fluoride (fluoroberyllate) or pure oxide (phosphate) glass. This is true despite the preponderance of fluorine over oxygen ions in the fluorophosphate system (about 7:1), and remains true even when measurements are delayed several radiative lifetimes after the flash to further suppress any contribution from shorter-lived states. It can be shown, however, that the probability of coordination by a single-anion species is relatively low. On purely electrostatic considerations (given the composition of the fluorophosphate), fewer than 10% of the Nd^{3+} ions should have no oxygens in the primary coordination sphere, and only one in 10^5 should have no fluorines. Even more important, the excitation wavelength ranges of the fluoroberyllate and phosphate overlap, indicating that in certain structures even fully fluorided and fully oxided Nd^{3+} ions can be excited at the same energy. This must be even more significant in the case of mixed coordination.

ACKNOWLEDGMENTS

The work at GTE Laboratories was supported in part by Lawrence Livermore Laboratory. The work at Livermore was funded under the auspices of the U.S. Department of Energy Materials Sciences Program and under Department of Energy Contract No. W7405-ENG. 48. We gratefully acknowledge the support of these agencies. We also thank B. W. Hawkins and J. Walsh for recording much of the FLN spectra, R. A. Saroyan and J. E. Lynch for recording absorption spectra and determining the Judd-Ofelt intensity parameters, and D. H. Blackburn of the National Bureau of Standards for melting the glass samples.

[1]A. Szabo, Phys. Rev. Lett. 25, 924 (1970); 27, 323 (1971).
[2]L. A. Riseberg, Phys. Rev. Lett. 28, 789 (1972); Solid State Commun. 11, 469 (1972); Phys. Rev. A 7, 671 (1973).
[3]N. Motegi and S. Shionoya, J. Lumin. 8, 1 (1973).
[4]P. Avouris, A. Campion, and M. A. El-Sayed, Chem. Phys. Lett. 50, 9 (1977); J. Chem. Phys. 67, 3397 (1977).
[5]C. Brecher and L. A. Riseberg, Phys. Rev. B 13, 81 (1976); C. Brecher, L. A. Riseberg, and M. J. Weber, *Proceedings of the Twelfth Rare Earth Research Conference, 1976* (University of Denver, Denver, 1976), Vol. I, p. 351.
[6]M. J. Weber, J. Hegarty, and D. H. Blackburn, in *Boron in Glass and Glass Ceramics* (Plenum, New York, to be published).
[7]C. Brecher and L. A. Riseberg (unpublished).
[8]T. Kushida and E. Takushi, Phys. Rev. B 12, 824 (1975).
[9]P. M. Selzer, D.L. Huber, D. S. Hamilton, W. M. Yen, and M. J. Weber, Phys. Rev. Lett. 36, 813 (1976); Proceedings of the Conference on Structure and Excitations of Amorphous Solids, Williamsburg, Virginia, March, 1976 (unpublished).
[10]C. Brecher, L. A. Riseberg, and M. J. Weber, Appl. Phys. Lett. 30, 475 (1977).
[11]M. J. Weber, *Proceedings of the Seventh International Conference on Amorphous and Liquid Semiconductors, Edinburgh, 1977* (North-Holland, Amsterdam, 1978), p. 645.
[12]C. B. Layne, W. H. Lowdermilk, and M. J. Weber, Phys. Rev. B 16, 10 (1977).
[13]W. F. Krupke, IEEE J. Quantum Electron. QE-10, 450 (1974).
[14]R. R. Jacobs and M. J. Weber, IEEE J. Quantum Electron. QE-12, 102 (1976).
[15]R. Reisfeld, Struct. Bonding 22, 123 (1975).
[16]E. M. Dianov, A. Ya. Karasik, A. A. Kut'enkov, V. B. Neustruev, and I. A. Shcherbakov, Sov. J. Quantum Electron. 6, 90 (1976).
[17]C. B. Layne, W. H. Lowdermilk, and M. J. Weber, IEEE J. Quantum Electron. QE-11, 798 (1975).
[18]C. B. Layne and M. J. Weber, Phys. Rev. B 16, 3259 (1977).
[19]C. B. Layne (private communication).
[20]M. J. Weber, J. A. Paisner, S. S. Sussman, W. M. Yen, L. A. Riseberg, and C. Brecher, J. Lumin. 12/13, 729 (1976).